A substorm-dependent negative limit of non-eclipse surface charging of a Chinese geosynchronous satellite

Zhiyi Fu[1,2,3], Zhenpeng Su[1,2,3*], Bin Miao[1,2,3], Zhiyong Wu[1,2,3], Yiren Li[1,2,3], Kai Liu[1,2,3], Xu Shan[4*], and Yuming Wang[1,2,5]

[1]Deep Space Exploration Laboratory/School of Earth and Space Sciences, University of Science and Technology of China, Hefei 230026, China

[2]CAS Center for Excellence in Comparative Planetology/CAS Key Laboratory of Geospace Environment/Mengcheng National Geophysical Observatory, University of Science and Technology of China, Hefei 230026, China

[3]Collaborative Innovation Center of Astronautical Science and Technology, Harbin 150001, China

[4]Hefei National Research Center for Physical Sciences at the Microscale, Department of Modern Physics, University of Science and Technology of China, Hefei 230026, China

[5]Hefei National Laboratory, University of Science and Technology of China, Hefei 230026, China

Key Points:

- Negative surface charging potentials are inferred from ion energy spectrograms for a Chinese geosynchronous navigation satellite.
- Non-eclipse extreme negative surface charging occurs primarily at the magnetic local times from 0.5 to 9.
- Non-eclipse surface charging potentials have a negative limit determined by substorm strength.

Corresponding author: Zhenpeng Su and Xu Shan, szpe@mail.ustc.edu.cn and xshan@ustc.edu.cn

Abstract

Surface charging is one of the most common causes of spacecraft anomalies. When and to what potential the spacecraft is charged are two important questions in space weather. Here, for a Chinese geosynchronous navigation satellite, we infer the extreme negative surface charging potentials from the ion differential fluxes measured by a low-energy ion spectrometer. Without the solar eclipse effect away from the midnight, the charging potentials are found to have a negative limit which is determined by the maximum SuperMAG electrojet index in the preceding 2 hr. Such an empirical relation can be reasonably explained by the dependence of 1–50 keV electron fluxes on substorm strength. Similar relations may also exist for other inner magnetospheric spacecraft in the non-eclipse region, which would be useful for spacecraft engineering and space weather alerts.

Plain Language Summary

Spacecraft charging is the charging of spacecraft surfaces or components relative to the surrounding space plasma. Compared to internal charging, surface charging is able to cause more serious spacecraft anomalies. When and to what potential the spacecraft is charged are two important questions in space weather. For a Chinese navigation satellite in the geosynchronous orbit, we show that the non-eclipse charging potentials have a negative limit determined by the maximum SuperMAG electrojet index in the preceding 2 hr. Such an empirical relation can be reasonably explained by the dependence of 1–50 keV electron fluxes on substorm strength. For other magnetospheric spacecraft, similar relations may also exist and would be useful for spacecraft engineering and space weather alerts.

1 Introduction

Spacecraft charging is the charging of spacecraft surfaces or components relative to the surrounding space plasma. This can lead to discharges and even catastrophic anomalies (Rosen, 1976; Reagan et al., 1983; Lanzerotti et al., 1998; Choi et al., 2011; Loto'aniu et al., 2015; Ganushkina et al., 2021). When and to what potential the spacecraft is charged are two important questions in space weather.

In general, spacecraft charging can be classified into surface and internal charging (Reagan et al., 1983; Czepiela et al., 2000). Compared to internal charging, surface charg-

ing is able to cause more serious spacecraft anomalies (Koons et al., 1999; Choi et al., 2011; Matéo-Vélez et al., 2018; Ganushkina et al., 2021). The surface charging is a result of the imbalance between currents exiting and entering the surface (Berry Garrett, 1981; Lai & Tautz, 2006a). In the environmental plasma of thermal equilibrium, compared to ions, electrons have much larger velocities and are easier to attach to the surface (Reagan et al., 1983; Lai & Della-Rose, 2001; Lai, 2003). In the inner magnetosphere, the enhancements of electrons with energies above keV have been found to cause the high negative surface charging (Olsen, 1983; Mullen et al., 1986; Lai & Tautz, 2006b; Sarno-Smith et al., 2016). These electrons are primarily injected by substorms into the region from midnight to dawnside (DeForest & McIlwain, 1971; Moore et al., 1981; Meredith et al., 2004; Forsyth et al., 2016; Ganushkina et al., 2021). When solar photons with sufficiently high energies strike the surface materials, photoelectrons are emitted from the surface (Grard et al., 1983). In the eclipse region where the sunlight has been blocked by the Earth, spacecraft are more likely to be charged to extremely high negative potentials (Mullen et al., 1981; Berry Garrett, 1981; Sarno-Smith et al., 2016; Matéo-Vélez et al., 2018). Given the cascading causal relationships of substorms, energetic electrons, and negative surface charging described above, a natural question arises to as whether it is possible to develop an empirical relation between the non-eclipse surface charging potential and the substorm activity strength.

In this study, we concentrate on the surface charging of a Chinese navigation satellite in the geosynchronous orbit. We show that the surface charging potentials inferred from the measurements of ion differential fluxes by the Low Energy Ion Spectrometer (LEIS) (Shan et al., 2023a, 2023b) have a substorm-dependent negative limit in the non-eclipse region.

2 Inference of Surface Charging Potentials

Onboard the satellite, the LEIS instrument can measure the ion fluxes in the energy range of 0.05–25 keV/q over a large field of view of 360° azimuthal angles and 90° elevation angles (Shan et al., 2023a, 2023b). The elevation angles of incident ions are determined by the deflector voltages, and the incident ions of different azimuthal angles are counted at 16 channels (numbered from Ch00 to Ch15). We here use the data from Ch05 whose view was not obstructed by other spacecraft components. These data have a time resolution Δt of 20 s and a relative energy resolution $\frac{\Delta E_\mathrm{k}}{E_\mathrm{k}}$ of 8.5%.

Figure 1 shows an example of ion differential fluxes recorded by Ch05 of LEIS from 15:00 UT to 21:00 UT on 14 October 2021. In the spectrogram, the extreme enhancement of ion fluxes in a narrow range of energy bins appears like a bright yellow line, which is an indicator of negative surface charging (DeForest, 1972; Sarno-Smith et al., 2016). The low-energy ions are accelerated by the negative potentials when approaching the spacecraft and then the recorded high-energy ion fluxes exhibit an unusual enhancement. Given that the background ions are mainly protons, the charging potential absolute $|U_{\rm s}|$ approximately equals the energy $E_{\rm k}$ of bright line divided by the unit charge e. In this event, the charging potential absolute $|U_{\rm s}|$ reached ∼3900 V near the midnight around 16:19 UT and fell to $\sim$ 400 V in the post-midnight region after 17:00 UT. As illustrated in the previous studies (Grard et al., 1983; Ferguson et al., 2015; Matéo-Vélez et al., 2018), the geosynchronous spacecraft experiences the solar eclipses around the midnight near the equinoxes. In this event, the solar eclipse may be the primary cause of extreme negative surface charging around 16:19 UT, and the substorm injection may be responsible for the rest charging.

We have developed an algorithm to automatically recognize the extreme charging events ($|U_{\rm s}| > 100$ V). We identify the energy bins forming the bright lines with the following two empirical criteria: differential fluxes $j(E_{\rm k}) > 10^8$ cm^{-2}s^{-1}sr^{-1}keV^{-1} and normalized gradients of ion count rates along the energy direction $\overline{C}(E_{\rm k}) > 0.7$. At the ith energy bin $E_{{\rm k},i}$, the normalized energy gradient $\overline{C}(E_{{\rm k},i})$ of the ion count rate n_i is written as

$$\overline{C}(E_{{\rm k},i}) = \frac{C(E_{{\rm k},i})}{\max\left(C(E_{{\rm k},j}),\ j=1,\ 2,\ 3,\cdots\right)}, \tag{1}$$

$$C(E_{{\rm k},i}) = \left|\frac{n_i - n_{i-1}}{\log E_{{\rm k},i} - \log E_{{\rm k},i-1}}\right|. \tag{2}$$

As exemplified in Figure 1, our algorithm can well identify the charging line. Using this algorithm, we have found 4068 extreme charging events from 24 September 2021 to 25 May 2023 (with a data gap related to the latch-up in the LEIS electronics from 09 May 2022 to 28 December 2022). These extreme charging events ($|U_{\rm s}| > 100$ V) are scattered over 133 days.

3 Surface Charging Magnitudes, Locations and Timings

Figure 2 shows the distribution of charging events in terms of magnitude, location, and time. As shown in Figure 2a, these charging events could be classified into two groups

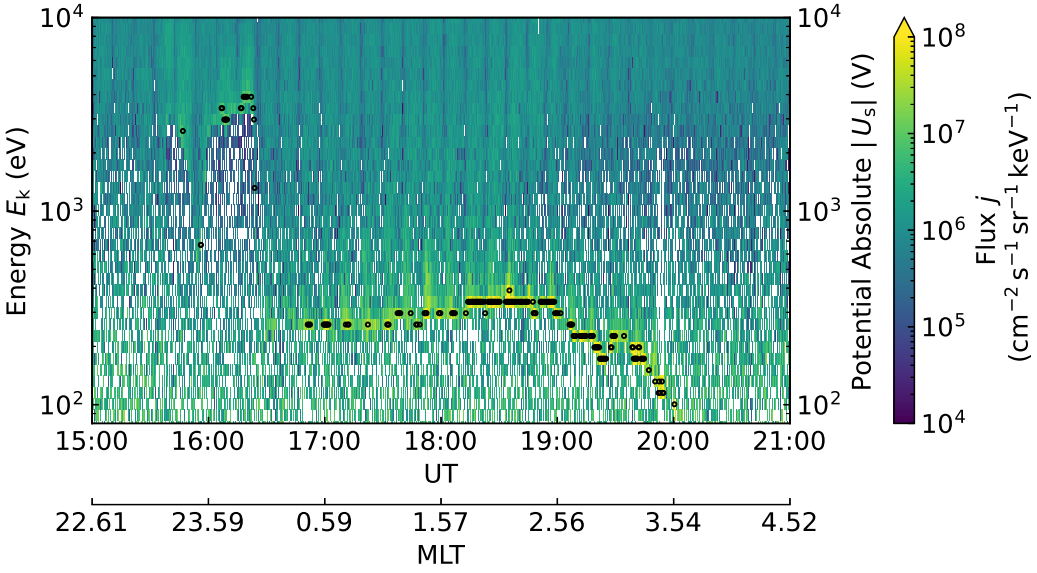

Figure 1. Ion differential fluxes j (color-coded) recorded by Ch05 channel of LEIS from 15:00 UT to 21:00 UT on 14 October 2021. The black circles mark the negative surface charging events identified automatically.

according to their occurring magnetic local times (MLT). One group is located at MLT=22.5–0.5, whose potentials $|U_s|$ extend to 10^4 V. These extreme charging events with $|U_s| > 2\times10^3$ V gather near the equinoxes (Figure 2b) and could be triggered by the solar eclipses (Grard et al., 1983; Ferguson et al., 2015; Matéo-Vélez et al., 2018). In contrast, the other group has a lower charging potential limit and occurs primarily in the region counter-clockwise from MLT=0.5 to MLT=9. This group should be free from the solar eclipse effect and be directly related to the substorm injection. These spatial distribution characteristics of the eclipse and non-eclipse events are generally consistent with those for the Van Allen Probes (Mauk et al., 2013; Sarno-Smith et al., 2016). The significant MLT asymmetry of non-eclipse events should be a result of electron drift in the magnetosphere. A statistical study (Li et al., 2010) has shown that the MLT asymmetry of electron fluxes decreases with the increase of energies. These non-eclipse charging could be caused primarily by electrons with energies from keV to tens of keV (Li et al., 2010).

4 Substorm Dependent Negative Limit of Charging Potentials

The substorm activities are characterized by the SuperMAG electrojet (SME) index (Newell & Gjerloev, 2011). SME index is the SuperMAG generalization of the tra-

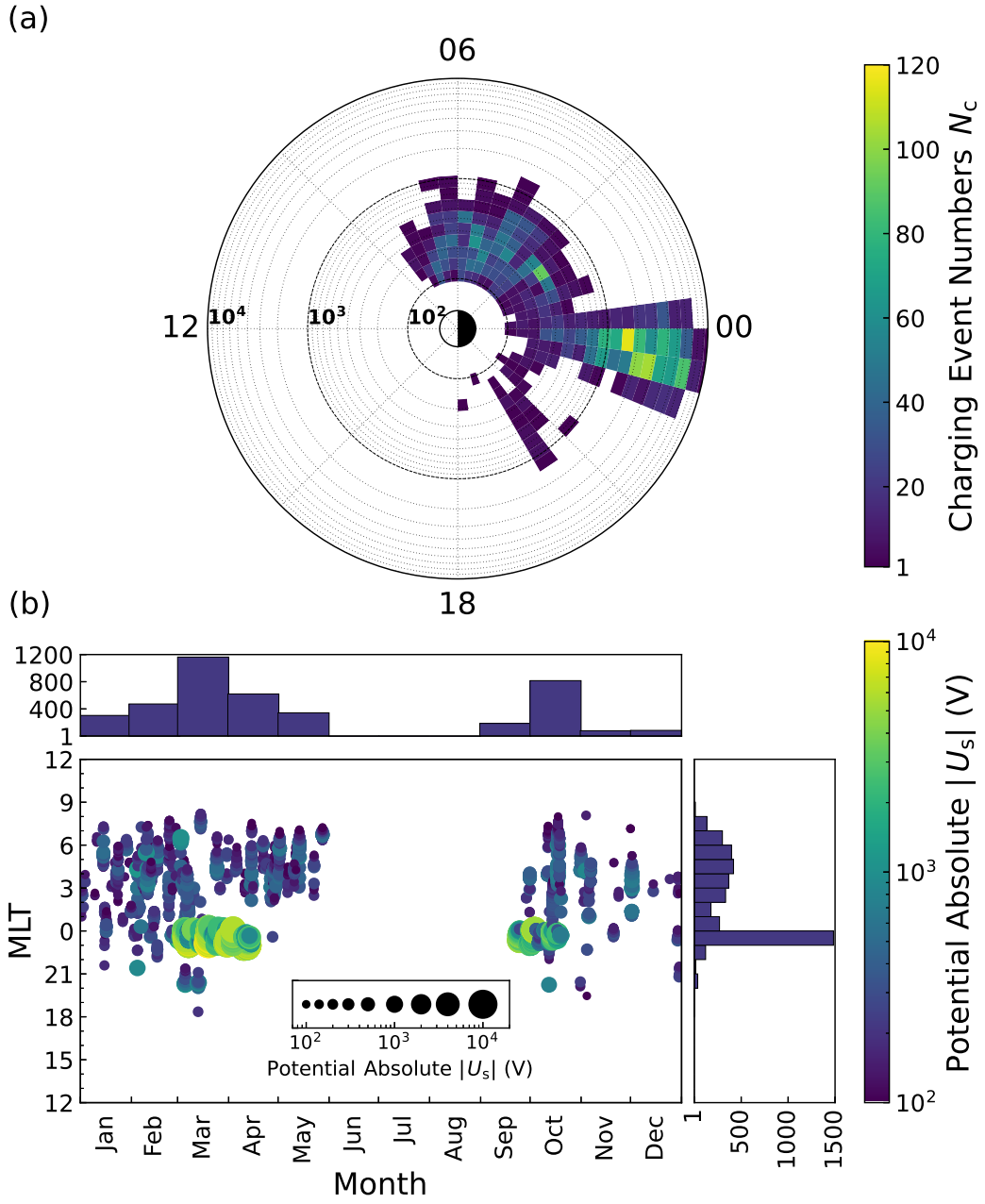

Figure 2. Magnitudes, locations, and timings of surface charging. (a) Extreme negative charging event number N_c (color-coded) as a function of potential absolute $|U_s|$ and magnetic local time (MLT). The radial direction represents $|U_s|$ and the azimuthal direction represents MLT. (b) Scatter plot of extreme negative charging events in the MLT-month plane, with the side panels represent the number of events contained within each interval. The color and size of each point are coded according to $|U_s|$. Note that our data has a gap approximately from June to August.

ditional auroral electrojet (AE) index. Different from AE based on the measurements of 12 ground-based magnetometer stations, SME is evaluated with more than 100 stations. Considering the drift and accumulation of substorm-injected electrons, we introduce SME*, the maximum SME in the preceding 2 hr. Figure 3 presents a scatter plot of 4068 charging events in the $|U_s|$−SME* plane. Near the midnight (MLT=22.5–0.5), the charging potentials $|U_s|$ appear to be distributed irregularly. This feature is reasonable because the solar eclipse effect is independent of substorm strength. In contrast, away from the midnight, the non-eclipse events are related to the substorm-injected electrons. The corresponding charging potentials $|U_s|$ have an upper limit $|\overline{U_s}|$ controlled by SME*. Specifically, when SME*$<$ 800 nT, the logarithm of potential upper limit $\log|\overline{U_s}|$ increases approximately linearly with SME*; when SME*$>$ 800 nT, $|\overline{U_s}|$ visually reaches a saturation level of 1.3×10^3 V. Overall, we can obtain a simple relation between $|\overline{U_s}|$ and SME*

$$|\overline{U_s}| = 10^{c_1 \tanh\frac{\mathrm{SME}^*-c_2}{c_3}+c_4}\ \mathrm{V}, \tag{3}$$

with the fitting parameters c_1, c_2, c_3, and c_4 and the determination coefficient R^2 listed in Table 1.

Table 1. Fitting parameters and determination coefficients of the $|\overline{U_s}|$–SME* and $\overline{j}$–SME* relations defined in Equations (3) and (4).

Name		c_1	c_2 (nT)	c_3 (nT)	c_4	R^2
Charging Potential		0.34380	495.03	198.90	2.7223	0.96941
Electron Flux	1 keV	0.021213	439.27	266.95	0.81318	0.98872
	10 keV	0.75240	-1258.9	686.99	0.0023428	0.94154
	50 keV	0.046832	196.18	291.53	0.65568	0.98295

The $|\overline{U_s}|$–SME* relation (3) described above can be reasonably explained by the substorm-dependence of energetic electron fluxes. Figure 4 shows the SME*-dependent distribution of 1, 10, and 50 keV electron fluxes j measured by the Van Allen Probes (Funsten et al., 2013; Blake et al., 2013; Spence et al., 2013) from MLT=0 to MLT=9 near the geosynchronous orbit during the time range from November 2012 to July 2019. We have divided these data into 8 intervals of SME* and then calculate the geometric mean $\overline{j}$ in

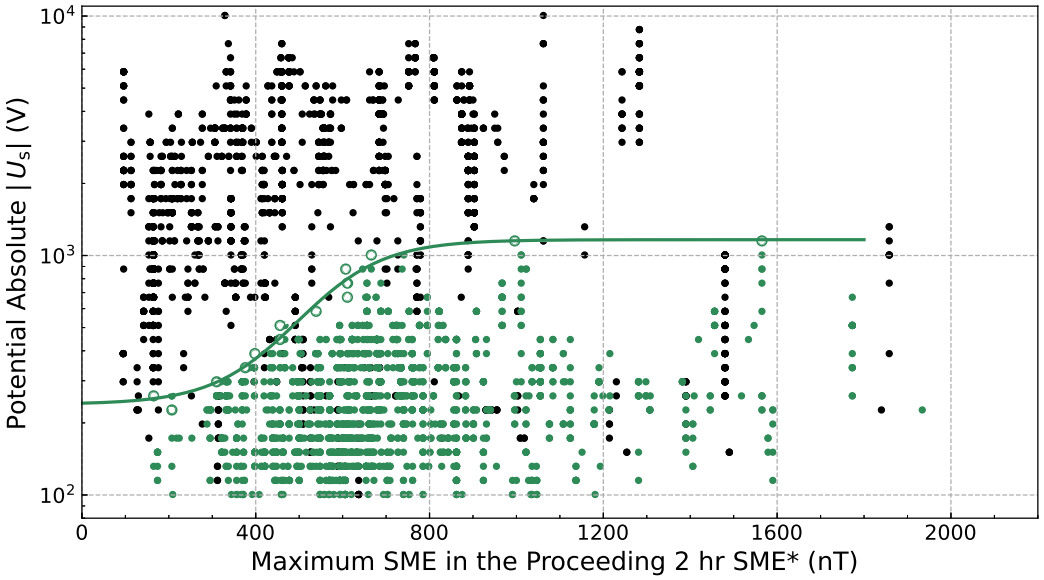

Figure 3. Scatter plot of extreme negative surface charging events in the SME*–$|U_s|$ plane, with the black color for the eclipse events (MLT=22.5–0.5) and the green color for the non-eclipse events (MLT=18–22.5 and MLT=0.5–9). The green line represents a nonlinear fit to the upper potential limit (green circles) of non-eclipse events.

each interval. It is obvious that, at every energy bin, $\overline{j}$ exhibits a SME*-dependence analogous to $|\overline{U_s}|$. Specifically, there is a monotonic increase of $\overline{j}$ when SME*$<$ 800 nT and a saturation of $\overline{j}$ when SME*$>$ 800 nT. Similar to $|\overline{U_s}|$, $\overline{j}$ can be fitted to a SME*-dependent function

$$\overline{j} = 10^{c_1 \tanh \frac{\mathrm{SME}^* - c_2}{c_3} + c_4} \ \mathrm{cm}^{-2}\mathrm{s}^{-1}\mathrm{sr}^{-1}\mathrm{keV}^{-1}, \tag{4}$$

with the fitting parameters and determination coefficients listed in Table 1.

5 Summary

This study sets out to develop an empirical relation between substorm strength and spacecraft surface charging potential in the non-eclipse region. For the Chinese satellite in the geosynchronous orbit, we infer the extreme negative charging potentials from the charging lines in the ion energy spectrograms measured by the LEIS instrument. The 4068 charing events with the potential absolutes $|U_s| > 100$ V can be classified into two groups: (1) the events close to the midnight, whose charging potentials have been affected by the solar eclipses near the equinoxes, and (2) the other events away from the midnight,

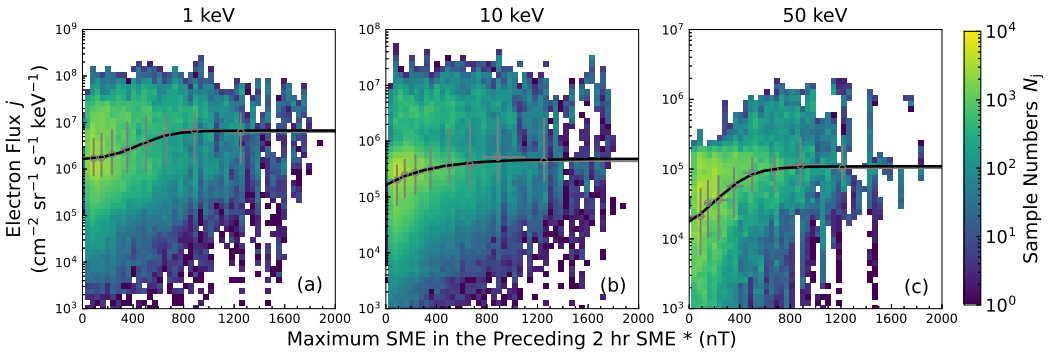

Figure 4. SME*-dependent electron differential fluxes j at (a) 1, (b) 10, and (c) 50 keV measured by the Van Allen Probes from MLT=0 to MLT=9 near the geosynchronous orbit during the time range from November 2012 to July 2019. These data have been divided into 8 intervals of SME*: 0–120 nT, 120–190 nT, 190–300 nT, 300–430 nT, 430–590 nT, 590–760 nT, 760–1100 nT and 1100–2000 nT. In each SME* interval (gray horizontal line), the geometric mean $\overline{j}$ (gray circle) and the corresponding upper and lower quartiles (gray horizontal line) have been calculated. The black lines represent a nonlinear fit to the obtained geometric means of electron fluxes.

whose charging potential absolutes have an upper limit $|\overline{U_s}|$ determined by the maximum SuperMAG electrojet index in the preceding 2 hr SME*. This simple $|\overline{U_s}|$-SME* relation for the non-eclipse events can be reasonably explained by the dependence of 1–50 keV electron fluxes on SME*. Spacecraft charging depends on the geometry and material properties of the spacecraft, as well as its orbital characteristics. For other inner magnetospheric spacecraft in the non-eclipse region, similar relations between the negative charging limit and the substorm strength may also exist. These empirical relations would be useful for spacecraft engineering and space weather alerts.

Open Research

LEIS data are available at http://space.ustc.edu.cn/dreams/leis/. Van Allen Probes data are available at https://spdf.gsfc.nasa.gov/pub/data/rbsp/. SME index is available at https://supermag.jhuapl.edu/.

Acknowledgments

We acknowledge all the collaborators from the Shandong Institute of Space Electronic Technology and China Academy of Space Technology for their help in the fabrication and environmental tests of LEIS. We acknowledge ECT teams for the use of Van Allen Probes data, and acknowledge the SuperMAG collaborators (http://supermag.jhuapl.edu/info/?page=acknowledg for the use of SME index. This work was supported by the National Natural Science Foundation of China grants 42188101, 42274198, and 42074222, and the Key Research Program of the Chinese Academy of Sciences grant ZDRE-KT-2021-3.

References

Berry Garrett, H. (1981, November). The Charging of Spacecraft Surfaces (Paper 1R1000). *Reviews of Geophysics and Space Physics*, *19*, 577. doi: 10.1029/RG019i004p00577

Blake, J. B., Carranza, P. A., Claudepierre, S. G., Clemmons, J. H., Crain, W. R., Dotan, Y., ... Zakrzewski, M. P. (2013, November). The Magnetic Electron Ion Spectrometer (MagEIS) Instruments Aboard the Radiation Belt Storm Probes (RBSP) Spacecraft. *Space Science Reviews*, *179*(1-4), 383-421. doi: 10.1007/s11214-013-9991-8

Choi, H.-S., Lee, J., Cho, K.-S., Kwak, Y.-S., Cho, I.-H., Park, Y.-D., ... Lee, D.-K. (2011, June). Analysis of GEO spacecraft anomalies: Space weather relationships. *Space Weather*, *9*(6), 06001. doi: 10.1029/2010SW000597

Czepiela, S. A., McManus, H., & Hastings, D. (2000, September). Charging of Composites in the Space Environment. *Journal of Spacecraft and Rockets*, *37*(5), 556-560. doi: 10.2514/2.3619

DeForest, S. E. (1972, January). Spacecraft charging at synchronous orbit. *Journal of Geophysical Research*, *77*(4), 651. doi: 10.1029/JA077i004p00651

DeForest, S. E., & McIlwain, C. E. (1971, January). Plasma clouds in the magnetosphere. *Journal of Geophysical Research*, *76*(16), 3587. doi: 10.1029/JA076i016p03587

Ferguson, D. C., Worden, S. P., & Hastings, D. E. (2015, September). The Space Weather Threat to Situational Awareness, Communications, and Positioning Systems. *IEEE Transactions on Plasma Science*, *43*(9), 3086-3098. doi: 10.1109/TPS.2015.2412775

Forsyth, C., Rae, I. J., Murphy, K. R., Freeman, M. P., Huang, C. L., Spence, H. E., ... Watt, C. E. J. (2016, July). What effect do substorms have on the content of the radiation belts? *Journal of Geophysical Research (Space Physics)*, *121*(7), 6292-6306. doi: 10.1002/2016JA022620

Funsten, H. O., Skoug, R. M., Guthrie, A. A., MacDonald, E. A., Baldonado, J. R., Harper, R. W., ... Chen, J. (2013, November). Helium, Oxygen, Proton, and Electron (HOPE) Mass Spectrometer for the Radiation Belt Storm Probes Mission. *Space Science Reviews*, *179*(1-4), 423-484. doi: 10.1007/s11214-013-9968-7

Ganushkina, N. Y., Swiger, B., Dubyagin, S., Matéo-Vélez, J. C., Liemohn, M. W., Sicard, A., & Payan, D. (2021, September). Worst-Case Severe Environments for Surface Charging Observed at LANL Satellites as Dependent on Solar Wind and Geomagnetic Conditions. *Space Weather*, *19*(9), e02732. doi: 10.1029/2021SW002732

Grard, R., Knott, K., & Pedersen, A. (1983, March). Spacecraft Charging Effects. *Space Science Reviews*, *34*(3), 289-304. doi: 10.1007/BF00175284

Koons, H. C., Mazur, J. E., Selesnick, R. S., Blake, J. B., & Fennell, J. F. (1999, July). *The Impact of the Space Environment on Space Systems.* Technical Report, AD-A376872; TR-99(1670)-1; SMC-TR-00-10 EL Segundo Technical Operations.

Lai, S. T. (2003, December). A critical overview on spacecraft charging mitigation methods. *IEEE Transactions on Plasma Science*, *31*(6), 1118-1124. doi: 10.1109/TPS.2003.820969

Lai, S. T., & Della-Rose, D. J. (2001, November). Spacecraft Charging at Geosynchronous Altitudes: New Evidence of Existence of Critical Temperature. *Journal of Spacecraft and Rockets*, *38*(6), 922-928. doi: 10.2514/2.3764

Lai, S. T., & Tautz, M. (2006b, September). High-level spacecraft charging in eclipse at geosynchronous altitudes: A statistical study. *Journal of Geophysical Research (Space Physics)*, *111*(A9), A09201. doi: 10.1029/2004JA010733

Lai, S. T., & Tautz, M. F. (2006a, October). Aspects of Spacecraft Charging in Sunlight. *IEEE Transactions on Plasma Science*, *34*(5), 2053-2061. doi: 10.1109/TPS.2006.883362

Lanzerotti, L. J., Breglia, C., Maurer, D. W., Johnson, G. K., & Maclennan,

C. G. (1998, January). Studies of spacecraft charging on a geosynchronous telecommunications satellite. *Advances in Space Research*, *22*(1), 79-82. doi: 10.1016/S0273-1177(97)01104-6

Li, W., Thorne, R. M., Nishimura, Y., Bortnik, J., Angelopoulos, V., McFadden, J. P., ... Auster, U. (2010, June). THEMIS analysis of observed equatorial electron distributions responsible for the chorus excitation. *Journal of Geophysical Research (Space Physics)*, *115*(1), A00F11. doi: 10.1029/2009JA014845

Loto'aniu, T. M., Singer, H. J., Rodriguez, J. V., Green, J., Denig, W., Biesecker, D., & Angelopoulos, V. (2015, August). Space weather conditions during the Galaxy 15 spacecraft anomaly. *Space Weather*, *13*(8), 484-502. doi: 10.1002/2015SW001239

Matéo-Vélez, J. C., Sicard, A., Payan, D., Ganushkina, N., Meredith, N. P., & Sillanpää, I. (2018, January). Spacecraft surface charging induced by severe environments at geosynchronous orbit. *Space Weather*, *16*(1), 89-106. doi: 10.1002/2017SW001689

Mauk, B. H., Fox, N. J., Kanekal, S. G., Kessel, R. L., Sibeck, D. G., & Ukhorskiy, A. (2013, November). Science Objectives and Rationale for the Radiation Belt Storm Probes Mission. *Space Science Reviews*, *179*(1-4), 3-27. doi: 10.1007/s11214-012-9908-y

Meredith, N. P., Horne, R. B., Thorne, R. M., Summers, D., & Anderson, R. R. (2004, June). Substorm dependence of plasmaspheric hiss. *Journal of Geophysical Research (Space Physics)*, *109*(A6), A06209. doi: 10.1029/2004JA010387

Moore, T. E., Arnoldy, R. L., Feynman, J., & Hardy, D. A. (1981, August). Propagating substorn injection fronts. *Journal of Geophysical Research*, *86*(A8), 6713-6726. doi: 10.1029/JA086iA08p06713

Mullen, E. G., Gussenhoven, M. S., & Garrett, H. B. (1981, July). *A worst case spacecraft environment as observed by SCATHA on 24 April 1979.*

Mullen, E. G., Gussenhoven, M. S., Hardy, D. A., Aggson, T. A., Ledley, B. G., & Whipple, E. (1986, February). SCATHA survey of high-level spacecraft charging in sunlight. *Journal of Geophysical Research*, *91*(A2), 1474-1490. doi: 10.1029/JA091iA02p01474

Newell, P. T., & Gjerloev, J. W. (2011, December). Substorm and magnetosphere

characteristic scales inferred from the SuperMAG auroral electrojet indices. *Journal of Geophysical Research (Space Physics)*, *116*(A12), A12232. doi: 10.1029/2011JA016936

Olsen, R. C. (1983, January). A threshold effect for spacecraft charging. *Journal of Geophysical Research Supplement*, *88*(A1), 493-499. doi: 10.1029/JA088iA01p00493

Reagan, J. B., Meyerott, R. E., Gaines, E. E., Nightingale, R. W., Filbert, P. C., & Imhof, W. L. (1983). Space charging currents and their effects on spacecraft systems. *IEEE Transactions on Electrical Insulation*, *EI-18*(3), 354-365. Retrieved from `https://api.semanticscholar.org/CorpusID:46669343` doi: 10.1109/TEI.1983.298625

Rosen, A. (1976, December). Spacecraft Charging by Magnetospheric Plasmas. *IEEE Transactions on Nuclear Science*, *23*(6), 1762-1768. doi: 10.1109/TNS.1976.4328575

Sarno-Smith, L. K., Larsen, B. A., Skoug, R. M., Liemohn, M. W., Breneman, A., Wygant, J. R., & Thomsen, M. F. (2016, February). Spacecraft surface charging within geosynchronous orbit observed by the Van Allen Probes. *Space Weather*, *14*(2), 151-164. doi: 10.1002/2015SW001345

Shan, X., Miao, B., Cao, Z., Sun, Z., Li, Y., Liu, K., ... Wang, Y. (2023a, May). First results of the low energy ion spectrometer onboard a Chinese geosynchronous satellite. *Science in China E: Technological Sciences*, *66*(5), 1378-1384. doi: 10.1007/s11431-022-2143-6

Shan, X., Miao, B., Cao, Z., Sun, Z., Li, Y., Liu, K., ... Wang, Y. (2023b, February). A low-energy ion spectrometer with large field of view and wide energy range onboard a Chinese GEO satellite. *Open Astronomy*, *32*(1), 210. doi: 10.1515/astro-2022-0210

Spence, H. E., Reeves, G. D., Baker, D. N., Blake, J. B., Bolton, M., Bourdarie, S., ... Thorne, R. M. (2013, November). Science Goals and Overview of the Radiation Belt Storm Probes (RBSP) Energetic Particle, Composition, and Thermal Plasma (ECT) Suite on NASA's Van Allen Probes Mission. *Space Science Reviews*, *179*(1-4), 311-336. doi: 10.1007/s11214-013-0007-5